PAPER www.rsc.org/dalton | Dalton Transactions

Mesomorphism of ionic allylpalladium(II) complexes containing pz^{R2}py as ligands and [BF$_4$]$^-$, [PF$_6$]$^-$ or [CF$_3$SO$_3$]$^-$ as counteranions†‡

Mari Carmen Torralba,[a] José Antonio Campo,[a] José Vicente Heras,[a] Duncan W. Bruce[b] and Mercedes Cano*[a]

Received 2nd February 2006, Accepted 15th May 2006
First published as an Advance Article on the web 30th May 2006
DOI: 10.1039/b601637e

The synthesis and thermal behaviour is reported of some ionic liquid-crystalline complexes formed when a mesogenic, two-chained, pyrazolylpyridine ligand is bound to a η^3-allylpalladium(II) fragment. The phase behaviour of the complexes is dominated by the formation of the SmA phase and, while the stability of the crystal phase appears to be controlled by intermolecular solid-state interactions, the stability of the liquid crystal phases is controlled by the length of the ligand alkoxy chains. Some of the complexes also show a complex polymorphism leading to the observation of double-melting behaviour.

1 Introduction

The study of metallomesogens, that is liquid crystals based on metal complexes, has developed significantly as a subject in the last twenty years and a wide range of different metals has been used in their construction, including d- and f-block elements.[1–6] Considering this work as a whole, it is clear that the majority of systems described might formally be regarded as coordination complexes, while a smaller number can be classified as organometallic (defined here as complexes containing M–C bonds including to CO and isonitriles).[7] Many organometallic systems derived from orthometallated imines and azo compounds bound to manganese(I), rhenium(I) and (particularly) palladium(II) and platinum(II) have been described, but there are fewer complexes where the organometallic moiety is coordinated with a hapticity of two or more (with the notable exception of ferrocene mesogens).[8] Examples include η^2-alkene complexes of Pt(II),[9] η^4-butadiene complexes of Fe(0),[10] and η^6-arene complexes of Cr(0).[11]

Recently, we reported the synthesis of Pd(II) mesogens containing an η^3-allyl group to which were also coordinated mesogenic pyrazoles. Previous work in our laboratory dealt with the studies of the mesomorphic properties of pyrazole ligands containing $C_6H_4OC_nH_{2n+1}$ as substituents at the 3- or at the 3- and 5-positions of the ring (Hpz^R and Hpz^{R2}, respectively) as well as that of some of their metal complexes.[12–17] Most of them behave as liquid crystal molecular materials, irrespective of whether mesomorphic (Hpz^{R2}) or non-mesomorphic (Hpz^R) ligands are used. So, for instance, it was interesting to note how the non-mesomorphic Hpz^R ligands induced liquid crystal behaviour on the complexes *t*-[Pd(Cl)$_2$(Hpz^R)$_2$], which exhibited a conventional rod-like molecular geometry.[14]

On these bases, the related mesogenic *N*,*N*′-bidentate 2-[3,5-bis(4-alkyloxyphenyl)pyrazol-1-yl]pyridine (pz^{R2}py) ligands were designed strategically and complexed with PdCl$_2$, giving rise to the expected [Pd(Cl)$_2$(pz^{R2}py)] compounds which also exhibited liquid crystal behaviour (Scheme 1).[18] Those results suggested us to consider that the unsymmetrical pz^{R2}py ligands can be used successfully to produce an elongated molecular shape and, at the same time, a lower symmetry of the complexes; both conditions prove to be useful in designing mesogens. By contrast, the related [Pd(Cl)$_2$(pz^{R}py)] complexes containing the non-mesomorphic pz^{R}py ligands bearing only one substituent at the 3-position of the pyrazole group, were not liquid-crystalline,[19] in agreement with the shortening of the molecular length in relation to that of the homologues containing pz^{R2}py ligands (Scheme 1). Surprisingly, when these *N*,*N*′-bidentate pz^{R}py ligands were coordinated to the [Pd(η^3-C$_3$H$_5$)]$^+$ fragment they gave rise to the new metallomesogenic [Pd(η^3-C$_3$H$_5$)(pz^{R}py)]$^+$.[19] Unfortunately, these complexes exhibited high clearing temperatures, giving rise to partial or full decomposition. Scheme 1 summarises the above results concerning the pyrazolylpyridine ligands and their complexes.

Following those precedents, we are now interested in proving that coordination of the longer and mesogenic pz^{R2}py ligands to the [Pd(η^3-C$_3$H$_5$)]$^+$ fragment should produce more adequate and hopefully more stable mesogenic derivatives. We wished to attain the possibility of improving the mesomorphic properties of these [Pd(η^3-C$_3$H$_5$)(pz^{R}py)]$^+$ systems by modifying the rod-like molecular shape. So, we thought that by introducing a new substituent group at the 5-position of the pyrazole ring, the anisometric ratio between molecular length and width of the resulting [Pd(η^3-C$_3$H$_5$)(pz^{R2}py)]$^+$ complexes should be increased in relation to that of those containing pz^{R}py ligands, so favouring the mesomorphic properties.

On the other hand, mesomorphism on palladium complexes containing bidentate ligands has been restricted to that of neutral cyclopalladated $\overline{\mathrm{N}(sp^2)\text{–}\mathrm{Pd}\text{–}\mathrm{C}}(sp^2)$ species,[20–26] and some others produced by coordination of several *N*,*N*-coordinated bipyridine-type ligands towards PdCl$_2$.[27] In addition, ionic mesogenic palladium derivatives have scarcely been reported.[28–31]

By contrast, linear two-coordinated cationic silver complexes with alkoxystilbazoles have been studied extensively,[32] their liquid crystal behaviour depending on the anion and

---

[a] *Departamento de Química Inorgánica I, Facultad de Ciencias Químicas, Universidad Complutense, E-28040, Madrid, Spain. E-mail: mmcano@quim.ucm.es; Fax: +34-91-3944352*

[b] *Department of Chemistry, University of York, Heslington, York, UK YO10 5DD*

† Dedicated to Dr J. A. Abad (University of Murcia, Spain) with occasion of his retirement.

‡ Electronic supplementary information (ESI) available: Spectroscopic data of all compounds, microphotographs from SmA mesophases of **I**$_{16}$ and **II**$_{18}$, and seven selected DSC traces. See DOI: 10.1039/b601637e

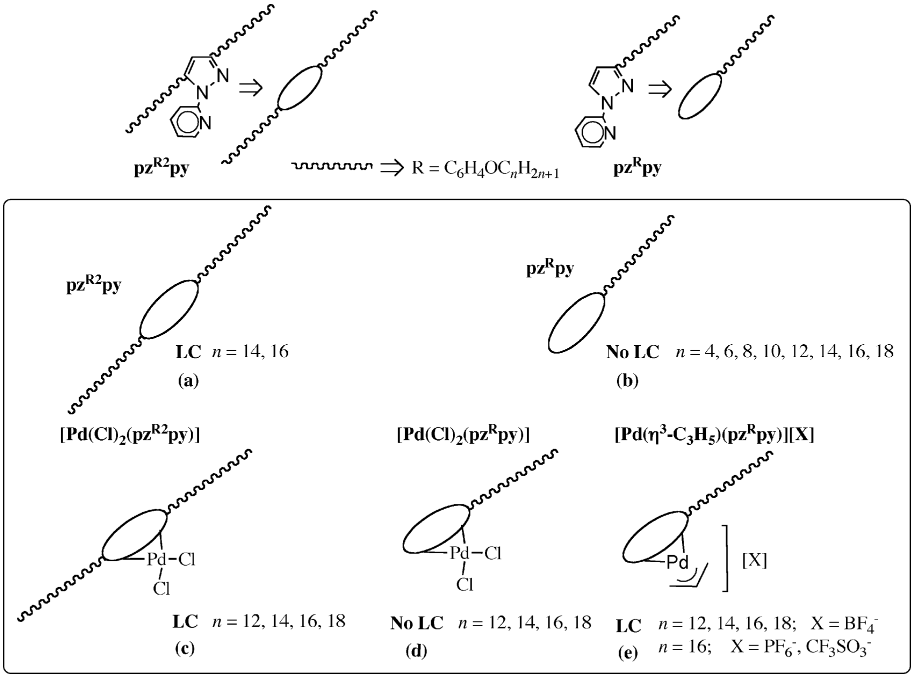

Scheme 1 Schematic molecular representation of the pz^{R2}py (a) and pz^{R}py (b) ligands, and their complexes: [Pd(Cl)$_2$(pz^{R2}py)] (c), [Pd(Cl)$_2$(pz^{R}py)] (d) and [Pd(η^3-C$_3$H$_5$)(pz^{R}py)][X] (e).

the number and length of alkoxy chains, among other factors.

In the present work we describe the preparation, characterisation and thermal study of a family of ionic complexes [Pd(η^3-C$_3$H$_5$)(pz^{R2}py)][X] (pz^{R2}py = 2-[3,5-bis(4-alkyloxyphenyl)pyrazol-1-yl]pyridine, R = $C_6H_4OC_nH_{2n+1}$, n = 10 (dp), 12 (ddp), 14 (tdp), 16 (hdp), 18 (odp)), X = BF_4^- (**I**), PF_6^- (**II**) and $CF_3SO_3^-$ (**III**). Scheme 2 shows the complexes studied in this work including the nomenclature used. All complexes of these three classes containing chains with 14–18 carbon atoms and the compound with 12 carbon atoms at the chains and BF_4^- (**I**$_{12}$) have been proved to have liquid crystal properties.

This type of complexes constitute one of the few examples of ionic mesogenic palladium derivatives that contain unsymmetrical *N*,*N*′-bidentate ligands in a rigid five-membered metallocyclic core.

2 Experimental

2.1 Materials and physical measurements

All commercial reagents were used as supplied. The starting Pd-complex [Pd(μ-Cl)(η^3-C$_3$H$_5$)]$_2$ was purchased from Sigma-Aldrich

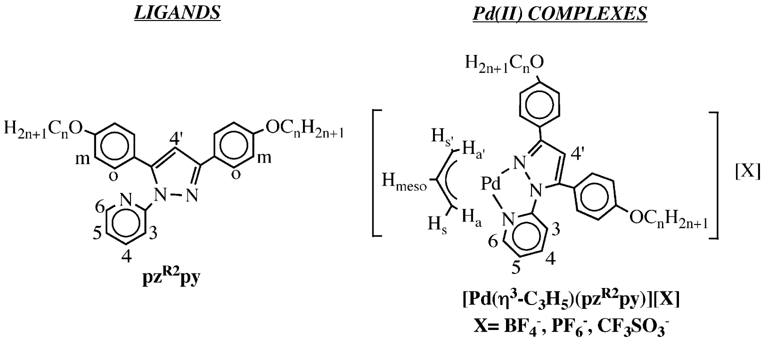

			BF$_4^-$	PF$_6^-$	CF$_3$SO$_3^-$
n = 10	**pz^{dp2}py**	*n* = 10	**I$_{10}$**		
n = 12	**pz^{ddp2}py**	*n* = 12	**I$_{12}$**	**II$_{12}$**	**III$_{12}$**
n = 14	**pz^{tdp2}py**	*n* = 14	**I$_{14}$**	**II$_{14}$**	**III$_{14}$**
n = 16	**pz^{hdp2}py**	*n* = 16	**I$_{16}$**	**II$_{16}$**	**III$_{16}$**
n = 18	**pz^{odp2}py**	*n* = 18	**I$_{18}$**	**II$_{18}$**	**III$_{18}$**

Scheme 2

and used as supplied. The 2-[3,5-bis(4-alkyloxyphenyl)pyrazol-1-yl]pyridine ($pz^{R2}py$) ligands ($R = C_6H_4OC_nH_{2n+1}$, n = 12, 14, 16, 18) were prepared as described previously.[18,33]

Elemental analyses for carbon, hydrogen, nitrogen and sulfur were carried out by the Microanalytical Service of Complutense University. IR spectra were recorded on a FTIR ThermoNicolet 200 or on a FTIR Nicolet Magna-550 spectrophotometers with samples as KBr pellets in the 4000–400 cm^{-1} region: vs (very strong), s (strong), m (medium), w (weak).

^1H NMR spectra were performed on a Bruker AC200, on a Bruker DPX-300 or on a Varian VXR-300 spectrophotometers (NMR Service of Complutense University) from solutions in $CDCl_3$. Chemical shifts δ are listed relative to TMS using the signal of the deuterated solvent as reference (7.26 ppm), and coupling constants J are in hertz. Multiplicities are indicated as s (singlet), d (doublet), t (triplet), m (multiplet), br (broad signal). The atomic numbering used in the assignment of the signals is shown in Scheme 2. The ^1H chemical shifts and coupling constants are accurate to ±0.01 ppm and ±0.3 Hz, respectively.

Phase studies were carried out by optical microscopy using an Olympus BX50 microscope equipped with a Linkam THMS 600 heating stage. The temperatures were assigned on the basis of optic observations with polarised light.

Measurements of the transition temperatures were made using a Perkin Elmer Pyris 1 differential scanning calorimeter with the sample (1–4 mg) sealed hermetically in aluminium pans and with a heating or cooling rate of 5–10 K min^{-1}.

The X-ray diffractograms at variable temperature were recorded on a Panalytical X'Pert PRO MPD diffractometer in a θ–θ configuration equipped with a Anton Paar HTK1200 heating stage (X-Ray Diffraction Service of Complutense University).

2.2 Preparation of 2-[3,5-bis(4-decyloxyphenyl)pyrazol-1-yl]pyridine ($pz^{dp2}py$)

The new ligand $pz^{dp2}py$ was prepared in a similar way used for analogous ligands.[18,33] This synthesis is based on the condensation of the corresponding 1,3-bis(4-alkyloxyphenyl)propane-1,3-dione and 2-hydrazinopyridine in ethanol using an acidic media to increase the yield. Mp 68 °C. Yield: 36%. Elemental analyses: found: C 78.5, H 8.9, N 6.5%; calc. for $C_{40}H_{55}N_3O_2$: C 78.8, H 9.1, N 6.9%. Spectroscopic data are given as ESI.‡

2.3 Preparation of $[Pd(\eta^3\text{-}C_3H_5)(pz^{R2}py)][BF_4]$ ($R = C_6H_4OC_nH_{2n+1}$; n = 10 (I_{10}), 12 (I_{12}), 14 (I_{14}), 16 (I_{16}), 18 (I_{18}))

To a solution of $[Pd(\mu\text{-}Cl)(\eta^3\text{-}C_3H_5)]_2$ (100 mg, 0.273 mmol) in dry acetone (20 mL) was added $AgBF_4$ (106.3 mg, 0.546 mmol) under a nitrogen atmosphere. The mixture was stirred in the absence of light at least for 6 h and then filtered over Celite. The corresponding $pz^{R2}py$ (0.546 mmol) in acetone (40 mL) was added to the resulting colourless solution and allowed to stir for 24 h at room temperature under nitrogen. Then the solvent was removed *in vacuo* and the solid crystallised from dichloromethane—hexane leading to the precipitation of a colourless solid, which was filtered off, washed with hexane and dried *in vacuo*. Yields and analytical data are collected in Table 1. Spectroscopic data are given as ESI.‡

2.4 Preparation of $[Pd(\eta^3\text{-}C_3H_5)(pz^{R2}py)][X]$ ($X = PF_6^-$, $R = C_6H_4OC_nH_{2n+1}$; n = 12 (II_{12}), 14 (II_{14}), 16 (II_{16}), 18 (II_{18}); $X = CF_3SO_3^-$, $R = C_6H_4OC_nH_{2n+1}$; n = 12 (III_{12}), 14 (III_{14}), 16 (III_{16}), 18 (III_{18}))

Complexes **II** and **III** were prepared in a same way to that above described for the BF_4 derivatives **I**, but starting from $AgPF_6$ or $AgCF_3SO_3$. Yields and analytical data are collected in Table 1. Spectroscopic data are given as ESI.‡

3 Results and discussion

3.1 Synthetic studies

The syntheses of $[Pd(\eta^3\text{-}C_3H_5)(pz^{R2}py)][X]$ ($R = C_6H_4OC_nH_{2n+1}$, n = 10, 12, 14, 16, 18; $X = BF_4^-$ (I_{10-18}), PF_6^- (II_{12-18}), $CF_3SO_3^-$ (III_{12-18})) was carried out using a procedure similar to that used for the related complexes containing pz^Rpy. The complexes were obtained by reaction of $[Pd(\eta^3\text{-}C_3H_5)(acetone)_2][X]$ ($X = BF_4^-$, PF_6^-, $CF_3SO_3^-$), prepared *in situ* by reaction of the dimer $[Pd(\mu\text{-}Cl)(\eta^3\text{-}C_3H_5)]_2$ and AgX in acetone,[19,34] with the corresponding ligand $pz^{R2}py$ (Scheme 3).

3.2 Spectroscopic and structural characterisation

All the compounds were characterised by analytical and spectroscopic (IR and ^1H NMR) techniques (see Experimental section

Table 1 Yields and analytical data for the new complexes

			Elemental analysis: calc (found) (%)							
Compound		Yield (%)	C		H		N		S	
$[Pd(\eta^3\text{-}C_3H_5)(pz^{dp2}py)][BF_4]$	$\mathbf{I}_{10}$	62	61.2	(61.1)	7.2	(7.0)	5.0	(5.0)	—	—
$[Pd(\eta^3\text{-}C_3H_5)(pz^{ddp2}py)][BF_4]$	$\mathbf{I}_{12}$	65	62.7	(62.6)	7.6	(7.5)	4.7	(4.8)	—	—
$[Pd(\eta^3\text{-}C_3H_5)(pz^{tdp2}py)][BF_4]$	$\mathbf{I}_{14}$	70	64.0	(64.0)	8.0	(8.0)	4.5	(4.4)	—	—
$[Pd(\eta^3\text{-}C_3H_5)(pz^{hdp2}py)][BF_4]$	$\mathbf{I}_{16}$	67	65.2	(65.0)	8.4	(8.2)	4.2	(4.4)	—	—
$[Pd(\eta^3\text{-}C_3H_5)(pz^{odp2}py)][BF_4]$	$\mathbf{I}_{18}$	60	66.3	(66.2)	8.7	(8.5)	3.9	(3.9)	—	—
$[Pd(\eta^3\text{-}C_3H_5)(pz^{ddp2}py)][PF_6]$	$\mathbf{II}_{12}$	60	58.9	(58.6)	7.2	(6.9)	4.4	(4.5)	—	—
$[Pd(\eta^3\text{-}C_3H_5)(pz^{tdp2}py)][PF_6]$	$\mathbf{II}_{14}$	63	60.4	(60.2)	7.6	(7.4)	4.1	(4.3)	—	—
$[Pd(\eta^3\text{-}C_3H_5)(pz^{hdp2}py)][PF_6]$	$\mathbf{II}_{16}$	54	61.7	(61.4)	7.9	(7.8)	3.9	(4.0)	—	—
$[Pd(\eta^3\text{-}C_3H_5)(pz^{odp2}py)][PF_6]$	$\mathbf{II}_{18}$	58	62.9	(62.8)	8.2	(8.1)	3.7	(3.8)	—	—
$[Pd(\eta^3\text{-}C_3H_5)(pz^{ddp2}py)][CF_3SO_3]$	$\mathbf{III}_{12}$	70	59.9	(60.0)	7.1	(7.0)	4.4	(4.5)	3.3	(3.4)
$[Pd(\eta^3\text{-}C_3H_5)(pz^{tdp2}py)][CF_3SO_3]$	$\mathbf{III}_{14}$	81	61.3	(61.3)	7.5	(7.5)	4.1	(4.3)	3.2	(3.1)
$[Pd(\eta^3\text{-}C_3H_5)(pz^{hdp2}py)][CF_3SO_3]$	$\mathbf{III}_{16}$	76	62.6	(62.7)	7.9	(7.8)	3.9	(4.0)	3.0	(2.9)
$[Pd(\eta^3\text{-}C_3H_5)(pz^{odp2}py)][CF_3SO_3]$	$\mathbf{III}_{18}$	79	63.7	(63.7)	8.2	(8.0)	3.7	(3.8)	2.8	(2.9)

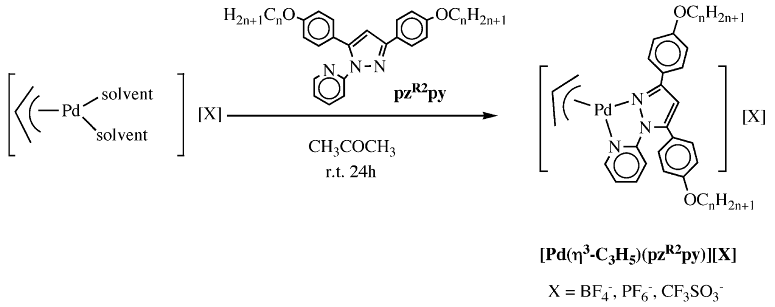

Scheme 3

and ESI‡), and all data agree with their proposed molecular formulation.

The IR spectra of the complexes in the solid state show the characteristic bands of the pyrazolylpyridine ligands scarcely modified upon coordination and confirmed the presence of the counteranions. It is interesting to mention the $\nu(C{=}N)$ band at *ca.* 1610 cm^{-1} from the pyrazolyl group as well as the characteristic bands for the different counteranions. So, for complexes **I**, a broad $\nu(B\text{–}F)$ band at *ca.* 1087–1052 cm^{-1} and $\delta(F\text{–}B\text{–}F)$ at *ca.* 518 cm^{-1} were observed from the BF_4^- counteranion. Analogously the $\nu(P\text{–}F)$ and $\delta(F\text{–}P\text{–}F)$ bands at *ca.* 844 and 558 cm^{-1}, respectively, from the PF_6^- counteranion were observed for complexes **II**. The spectra for complexes **III** with $CF_3SO_3^-$ as counteranion display the $\nu_d(SO_3)$ and $\nu(CF_3)$ bands overlapped at *ca.* 1260 cm^{-1} and the $\nu_s(SO_3)$ absorption at *ca.* 1029 cm^{-1}. The remaining bands are not certainly assigned because of the superposition with many others of the ligand.

The ^1H NMR spectra of the new complexes at room temperature in $CDCl_3$ solution (see ESI‡) show all the expected ligand signals slightly modified in each series of compounds. Some resonances appear to be overlapped or masked by other signals. The main difference in each series of compounds is the integration of the $(CH_2)_n$ signal. In all cases the ^1H NMR spectra display four groups of signals corresponding to the allyl, pyridyl, alkyloxyphenyl and pyrazolyl groups. For the allyl groups five resonances are observed corresponding to the *meso*, *syn* and *anti* protons, the last two being split in two signals due to the unsymmetric environment produced by the pyrazolylpyridine ligand. In general those *syn* and *anti* signals are very broad and overlapped each other or with the OCH_2 groups of the lateral chains showing the dynamic character of the allyl group. There are many examples in the literature describing the dynamic behaviour of allylpalladium complexes.[34–37] In the complexes studied herein, those signals were well resolved at room temperature in three compounds. So, for $\mathbf{I}_{14}$ and $\mathbf{I}_{16}$, four doublets were observed at 4.58 and 3.39 ppm (H*syn*), and 3.65 and 3.02 ppm (H*anti*), while for $\mathbf{II}_{16}$ these signals appear slightly shifted at higher field (4.43 and 3.40 ppm for H*syn*, 3.59 and 3.02 ppm for H*anti*). In same other cases these four signals could also be observed at lower temperatures (for instance, at -50 °C for $\mathbf{II}_{18}$), but not well resolved.

Concerning the pyridyl group, a doublet is observed for the H6 proton at *ca.* 8.89 ppm for complexes **I** and **III** (with BF_4^- and $CF_3SO_3^-$ as counteranions) being shifted upfield by *ca.* 0.15 ppm for the PF_6^- complexes (**II**). A similar behaviour is also shown for the H5 proton, this signal appearing partially masked by the H*o* protons of one C_6H_4 group. The signals corresponding to H3 and H4 protons are not modified by the presence of the different counteranions. It is of interest to mention that the H3 proton is shifted upfield with respect to the free ligand, whilst an opposite effect is observed for the H4, H5 and H6 protons.

The non-equivalence of the lateral substituents at the pyrazolyl ring remains upon coordination of the ligand, the spectra showing two signals for each type of their protons. One set of the H*o* protons of the C_6H_4 groups is shifted downfield with respect to the free ligand, while the other is shifted upfield. However, the two signals of the H*m* protons are slightly displaced at higher frequencies. The H4 signal of the pyrazolyl group is unchanged after coordination.

3.3 Structural studies

The relationship between chemical structure and mesomorphism has been investigated extensively in the field of liquid crystals, but drawing relationships between solid-state structures and mesomorphism is fraught with danger. Nonetheless, it is often instructive to look at these solid-state structures as there can be insights to be gained.

Following these considerations the X-ray structures of complexes $[Pd(\eta^3\text{-}C_3H_5)(pz^{bp2}py)][X]$ ($pz^{bp2}py$ = 2-[3,5-bis(4-butoxyphenyl)pyrazol-1-yl]pyridine; X = BF_4^- ($\mathbf{I}_4$), $CF_3SO_3^-$ ($\mathbf{III}_4$)) were solved and reported recently by us.[38] We consider it of interest to comment herein on the main relevant results as well as, for comparative purposes, those from the X-ray structure of the related complex $[Pd(\eta^3\text{-}C_3H_5)(pz^{hp}py)][BF_4]$ ($pz^{hp}py$ = 2-[3-(4-hexyloxyphenyl)pyrazol-1-yl]pyridine) (**IV**), which we also reported recently.[19] Firstly, it should be mentioned that the three complexes, $\mathbf{I}_4$, $\mathbf{III}_4$ and **IV**, exhibited a related molecular shape which can be defined as rod-like type with respect to the molecular length-to-width ratio (Fig. 1).

On a supramolecular level, the structure of $[Pd(\eta^3\text{-}C_3H_5)(pz^{hp}py)][BF_4]$ (**IV**) was consistent with a one-dimensional assembly produced through weak hydrogen-bonds between the counteranion BF_4^- and the cations $[Pd(\eta^3\text{-}C_3H_5)(pz^{hp}py)]^+$, so defining a zigzag chain almost parallel to the *b* axis.[19] In addition, extended hydrogen bonds hold together the chains in a two-dimensional network, in which molecules are arranged in bilayers with the chains interdigitated between them (Fig. 2).[19] Therefore we could deduce that the counteranion and the $pz^{hp}py$ ligand function as a source of hydrogen-bonds which generated a two-dimensional supramolecular assembly.

The literature of calamitic ionic liquid crystals[28] is dominated by the observation of SmA phases (although refs. 29 and 32

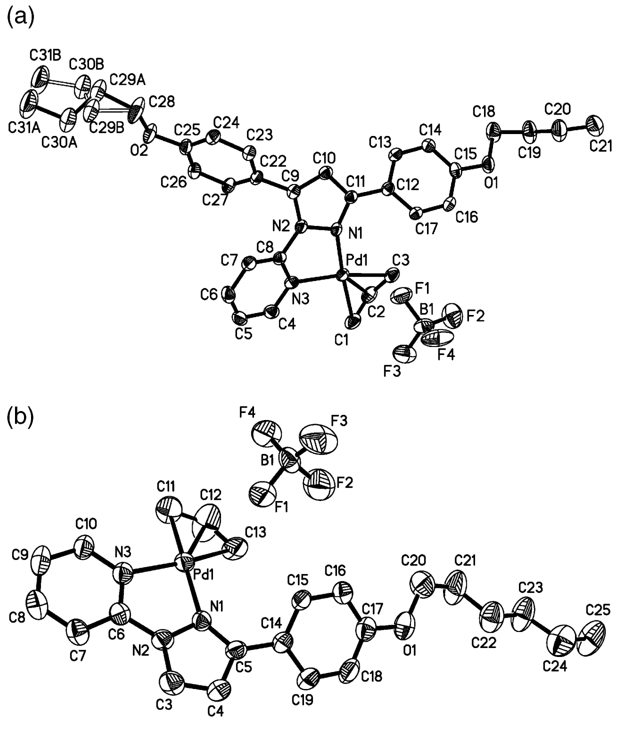

Fig. 1 (a) ORTEP plot of **I**$_4$,[38] and (b) ORTEP plot of **IV**,[19] in which a rod-like shape could be suggested (the structure of **III**$_4$ is similar to that of **I**$_4$)[38].

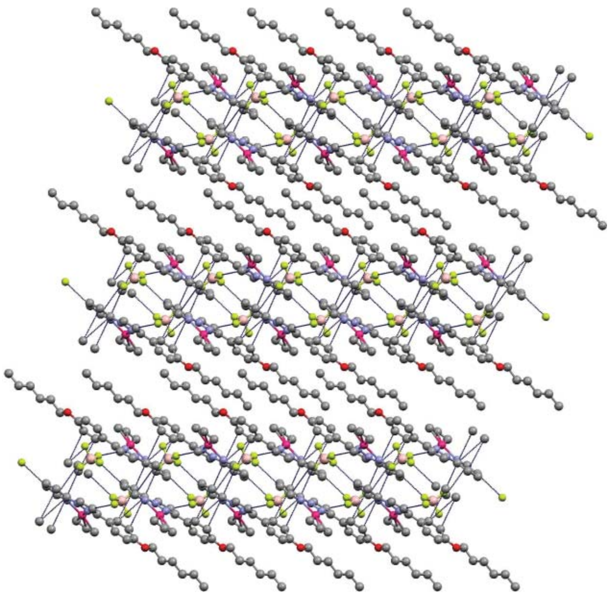

Fig. 2 Two-dimensional network of **IV**,[19] showing the interdigitation between bilayers.

contain exceptions from metallomesogen chemistry), and the formation of the smectic layers is undoubtedly promoted by intermolecular Coulombic attractions. In these complexes, the solid-state structure shows evidence of intermolecular hydrogen bonding, too, but consideration of the thermal behaviour of these complexes (*vide infra*) suggests that these forces influence the stability of the crystalline phases rather than the liquid-crystal phases.

As indicated earlier, the thermal behaviour of the complexes $[Pd(\eta^3\text{-}C_3H_5)(pz^{R}py)][BF_4]$ (R = $C_6H_4OC_nH_{2n+1}$, n = 6, 10, 12, 14, 16, 18) was investigated,[19] and those compounds with 12–18 carbon atoms in the chain exhibited SmA mesophases at high temperatures. The X-ray diffraction study at variable temperature of $[Pd(\eta^3\text{-}C_3H_5)(pz^{hdp}py)][BF_4]$ ($pz^{hdp}py$ = 2-[3-(4-hexadecyloxyphenyl)pyrazol-1-yl]pyridine), as a representative example, was consistent with a smectic type layered structure containing the molecules organised in interdigitated bilayers.[19] Therefore, there were some parallels between the arrangement in the mesophase and the structure observed in the crystalline solid state.

In our current work the complexes studied, $[Pd(\eta^3\text{-}C_3H_5)(pz^{R2}py)][X]$, are related to those containing $pz^{R}py$ as ligand and from the structural point of view should have a similar molecular shape. Thus, it was felt that the presence of two substituents at the 3- and 5-positions of the pyrazole ring should not modify the molecular skeleton appreciably or the solid-state arrangement involving the counteranions. However the potential two-dimensional supramolecular assembly could be more affected.

In fact, the X-ray single crystal structures of $[Pd(\eta^3\text{-}C_3H_5)(pz^{bp2}py)][X]$ (X = BF_4^- (**I**$_4$), $CF_3SO_3^-$ (**III**$_4$)) showed the presence of intermolecular H···O/F hydrogen-bonds between the cationic metal complexes and the counteranions, which were responsible for zigzag chains in a one-dimensional assembly.[38] In addition and concerning the counteranions, new H···O/F interactions involved interchain interactions that gave rise to layer-like arrangements, defining a two-dimensional network. In these layer-like structures, the flexible chains are interdigitated (Fig. 3).[38]

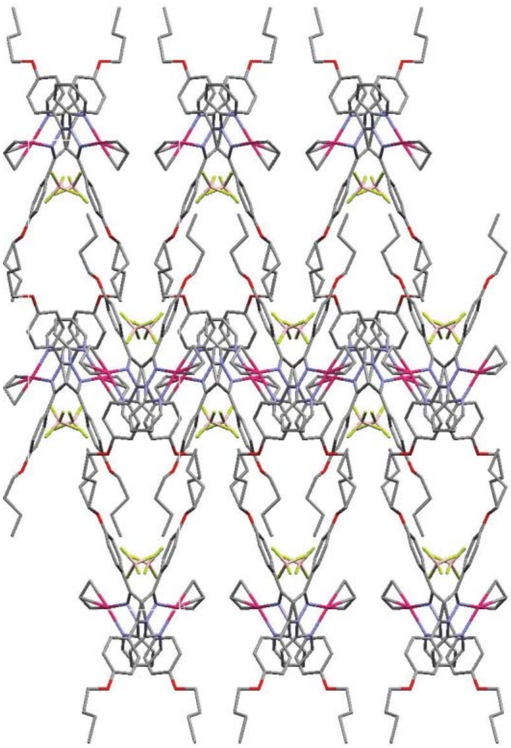

Fig. 3 Two-dimensional network of **I**$_4$,[38] showing the interdigitation of the chains between layers.

These structural features were similar to those of the related compound [Pd(η^3-C_3H_5)(pz^{hp}py)][BF_4], mentioned above, for which the hydrogen-bonding C–H···F interactions along (3.08 Å) and between (3.27 Å) chains[19] compared well with the values of 3.06 and 3.16 Å, respectively, observed in [Pd(η^3-C_3H_5)(pz^{bp2}py)][BF_4].[38] Then we deduce that, in cationic allylpalladium(II) complexes containing pz^{R2}py ligands, the 3,5-disubstitution at the pyrazole ring does not significantly modify the molecular assembly with respect to the analogous compounds containing only one substituent at the 3-position on the pyrazole, being in both cases described as the layer-like type in which the layers have formed a molecular arrangement defining a bilayer (Fig. 4). As a consequence, the number of chains interdigitated between layers is higher, leading to an increased filling of interlayer space.

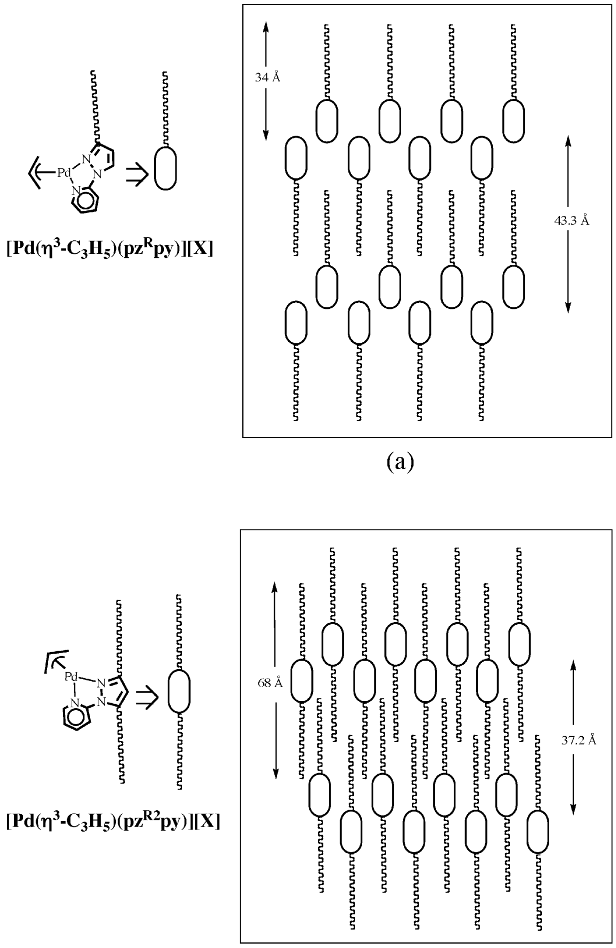

(a)

(b)

Fig. 4 Schematic representation of the bilayers of [Pd(η^3-C_3H_5)(pz^{R}py)][X] (a) and [Pd(η^3-C_3H_5)(pz^{R2}py)][X] (b) (the values of 43.3 (a) and 37.2 Å (b) correspond to the d_{001} spacing from the mesophases for [Pd(η^3-C_3H_5)(pz^{hdp}py)][BF_4] (**IV**) and [Pd(η^3-C_3H_5)(pz^{odp2}py)][BF_4] (**I**$_{18}$), respectively, and those of 34 (a) and 68 Å (b) to the calculated molecular length of the same compounds).

3.4 Thermal studies

The mesomorphism of the new complexes was studied by polarised light optical microscopy (POM), differential scanning calorimetry (DSC) and, in some cases, X-ray diffraction at variable temperature. The complete mesomorphism of complexes [Pd(η^3-C_3H_5)(pz^{R2}py)][X] (R = $C_6H_4OC_nH_{2n+1}$, n = 10, 12, 14, 16, 18; X = BF_4^- (**I**), PF_6^- (**II**), $CF_3SO_3^-$ (**III**)) is reported in Table 2.

Table 2 Phase properties of pz^{R2}py and [Pd(η^3-C_3H_5)(pz^{R2}py)][X] (**I**$_n$, **II**$_n$, **III**$_n$) determined by optical microscopy and DSC

Compound	Transition	$T/°C$	ΔH/kJ mol^{-1}
pz^{dp2}py	Cr → I	68.2	48.4
pz^{ddp2}py[a]	Cr → I	71.0	47.3
pz^{tdp2}py[a]	(I → SmA)	(44.1)	(−4.4)
pz^{hdp2}py[a]	(I → SmA)	(48.8)	(−5.7)
pz^{odp2}py[a]	Cr → I	52.1	59.6
I$_{10}$	Cr → Cr′	84	0.5
	Cr′ → I	126	37.6
I$_{12}$	Cr → Cr′	76	20.7
	Cr′ → Cr″ → I	148	48.1[b]
	(I → SmA)	(108)	(−1.3)
I$_{14}$	Cr → Cr′	78	6.2
	Cr′ → I	148	57.4
	(I → SmA)	(139)	(−1.8)
I$_{16}$	Cr → Cr′	76	13.8
	Cr′ → Cr″	142	
	Cr′ → SmA	145	56.2[b]
	SmA → I	157	2.0
I$_{18}$	Cr → Cr′	85	12.8
	Cr′ → SmA	137	56.2
	SmA → I	162	2.1
II$_{12}$	Cr → I	149	28.7
II$_{14}$	Cr → SmA	53	50.5
	SmA → Cr′	82	−15.2
	Cr′ → I	132	19.2
	(I → SmA)	(96)	(−1.5)
II$_{16}$	Cr → Cr′	48	10.6
	Cr′ → Cr″	86	9.0
	Cr″ → I	138	18.0
	(I → SmA)	(114)	(−1.9)
II$_{18}$	Cr → SmA	63	72.2
	SmA → Cr′	88	−12.7
	Cr′ → I	134	19.0
	(I → SmA)	(124)	(−1.9)
III$_{12}$	Cr → Cr′	88	5.7
	Cr′ → I	123	54.4
III$_{14}$	Cr → Cr′	98	8.3
	Cr′ → I	122	56.1
	(I → SmA)	(92)	(−1.5)
III$_{16}$	Cr → Cr′	113	9.0
	Cr′ → I	123	59.0
	(I → SmA)	(107)	(−1.8)
III$_{18}$	Cr → I	119	81.2
	(I → SmA)	(115)	(−2.1)
	SmA → Cr	47	−21.1
	Cr → SmA[c]	52	27.1
	SmA → I[c]	117	1.9

[a] Data from the pyrazolylpyridine ligands are given for comparative purposes and taken from ref. 18. [b] The peaks overlapped; combined enthalpy values are given. [c] Second heating.

The complexes **I–III** displayed only one type of mesophase, namely SmA mesophase, which was recognised on the basis of the optical texture, and so a typical oily streak texture was seen on cooling as well as batonnets that sometimes formed from the isotropic liquid (Fig. 5 and ESI,‡ Fig. S1). It is also worth noting that on a number of occasions, the texture appeared very strongly homeotropic. However, the overall thermal behaviour was not straightforward and is described now in more detail.

The shortest-chain homologue of complexes **I**, **I**$_{10}$, was not mesomorphic and simply melted to the isotropic state at 126 °C,

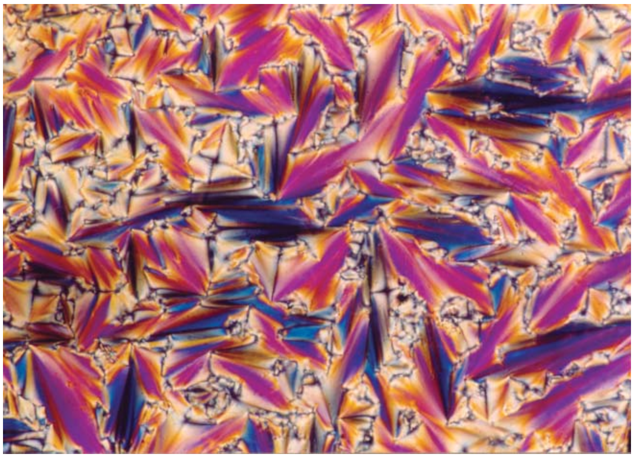

Fig. 5 Textures of the smectic A mesophase, observed on cooling, for $\mathbf{II}_{18}$ at 111 °C.

following a crystal–crystal transition at 84 °C. There was no evidence for any monotropic mesophase on cooling. Complex $\mathbf{I}_{12}$ also showed a crystal–crystal transition, this time at 76 °C, and then from around 140 °C there was a complex series of events. The DSC trace for this area is reproduced as Fig. 6 and shows what we believe to be a melting event followed rapidly by recrystallisation, followed by melting once more—this time to isotropic liquid. This assignment is based on the fact that the peak for the first melting event at about 147 °C, is not symmetric, and the steeper slope to high temperature rather suggests a catastrophic event consistent with recrystallisation. In the absence of an identifiable texture by microscopy, we were unable to assign the phase formed during this first melting event. When the isotropic phase was cooled, a readily identifiable SmA phase did form at 108 °C and persisted down to room temperature. Crystallisation was not observed and so on re-heating, both optical microscopy and DSC show a simple clearing event at 108 °C (see ESI,‡ Fig. S2). However, heating above this temperature showed a small, residual peak at about 146 °C which we attribute to the melting of some crystal that did re-form during a slow crystallisation process that took during the cooling and re-heating cycle. The third heat–cool cycle reproduces the second exactly.

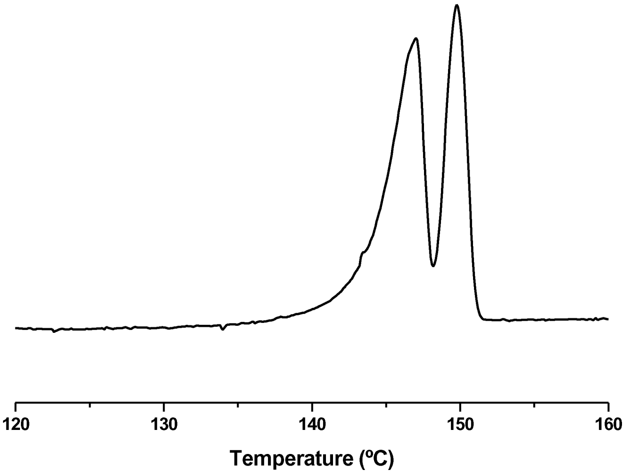

Fig. 6 DSC trace of $\mathbf{I}_{12}$ in the 120–160 °C range (first heating).

Complex $\mathbf{I}_{14}$ was a little more straightforward in that following a crystal–crystal transition at 78 °C, the complex melted directly to isotropic at 148 °C and a monotropic SmA phase formed at 139 °C, which persisted down to room temperature. Re-heating the SmA phase led to partial crystallisation, the remaining SmA areas cleared at 139 °C, while the crystalline parts melted to isotropic at 146 °C. Complex $\mathbf{I}_{16}$ also showed crystal–crystal transitions (76 and 142 °C) before melting into a SmA phase at 145 °C. The liquid-crystal phase persisted to 157 °C whereupon it cleared to give an isotropic liquid. Cooling the SmA phase was formed at 155 °C and persisted down to room temperature. On re-heating, partial crystallisation was observed, the solid parts re-melted at 146 °C while the SmA phase all cleared at 155 °C.

In common with all complexes containing octadecyloxy chains, $\mathbf{I}_{18}$ was the most straightforward and showed an enantiotropic SmA phase between 137 and 162 °C. Cooling once more led to the SmA phase at 162 °C, which was maintained down to room temperature, and on re-heating the SmA phase cleared at 162 °C.

For complexes **II**, once more the shortest-chain homologue was non-mesomorphic and $\mathbf{II}_{12}$ melted directly to the isotropic phase at 149 °C. Complex $\mathbf{II}_{14}$ was more interesting and melted at 53 °C to give a SmA phase. However, on further heating, the SmA phase crystallised at 82 °C, and the event is recorded clearly in the DSC trace (Fig. 7). Further heating to 132 °C led this new crystalline phase to melt to the isotropic liquid. On cooling, nothing was seen until 96 °C when the SmA phase re-formed, which persisted down below 50 °C. Reheating the sample showed that crystallisation had not occurred and all that was observed was the clearing transition of the SmA phase at 96 °C (ESI,‡ Fig. S3). The same pattern of behaviour was also seen for $\mathbf{II}_{18}$ where melting to SmA first occurred at 63 °C, with the SmA phase subsequently crystallising at 88 °C. The new crystalline phase melted to the isotropic liquid at 134 °C and cooling revealed a monotropic SmA phase at 124 °C. On cooling $\mathbf{II}_{18}$, crystallisation of the SmA phase was seen at 45 °C, but this was almost certainly incomplete as on re-heating, melting to SmA was observed at the slightly lower temperature of 52 °C with, more significantly, a much lower enthalpy of transition ($\Delta H = 72.2$ kJ mol^{-1} on the first heating compared with 28.4 kJ mol^{-1} on the second heating). The second heating showed no evidence of cold crystallisation of the SmA phase, which persisted to clearing at 123 °C. Complex $\mathbf{II}_{16}$ showed a pattern observed in the BF_4^- complexes in that following crystal–crystal transitions at 48 and 86 °C, the complex melted directly to the isotropic phase at 138 °C and showed a monotropic SmA phase at 114 °C, which persisted down to room temperature. DSC data for $\mathbf{II}_{16}$ and $\mathbf{II}_{18}$ are reproduced as Fig. S4 and S5, respectively (see ESI‡).

Complex $\mathbf{III}_{12}$ was non-mesomorphic simply melting at 123 °C, but the remaining three homologues showed a SmA phase. For $\mathbf{III}_{14}$ and $\mathbf{III}_{16}$, this was monotropic with melting points observed at 122 and 123 °C, respectively, and clearing points at 92 and 107 °C, respectively. Both complexes also showed two crystal polymorphs, and this behaviour was confirmed by observations made by DSC. On cooling, the mesophase in both compounds was maintained down below 50 °C with no evidence of crystallisation, indeed the viscosity suggested that the system had formed a smectic glass. Complex $\mathbf{III}_{18}$ melted directly to the isotropic phase at 119 °C and the SmA phase appeared monotropically at 115 °C. Crystallisation of the SmA phase was around 47 °C and

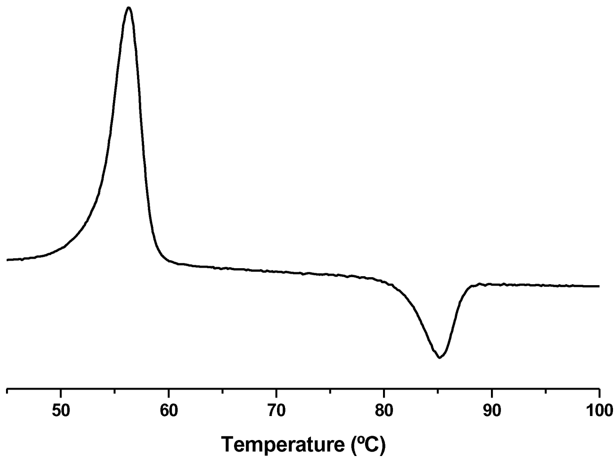

Fig. 7 DSC trace of **II**$_{14}$ in the 50–100 °C range (first heating).

on re-heating the solid, the compound melted directly to a SmA phase at 52 °C which persisted to the clearing point, measured at 117 °C on heating. Once more, these events were matched by corresponding events observed in the DSC trace. Thus, once more there are two accessible crystal forms giving rise to the SmA phase at different temperatures. DSC traces for **III**$_{14}$, **III**$_{16}$ and **III**$_{18}$ are shown as Fig. S6–S8 (see ESI‡).

In comparing the mesomorphism of the different series of materials, we first note that the decyloxy, dodecyloxy and octadecyloxy ligands were non-mesomorphic, while the tetradecyloxy and hexadecyloxy homologues showed monotropic SmA phases with clearing points below 50 °C (Table 2). Thus, complexation leads to materials whose mesophases are much more thermally stable, clearing in all cases at temperatures above 90 °C, and in some cases above 150 °C.

Within a given series of complexes, the melting points of the mesomorphic homologues are relatively invariant with chain length (*e.g.* between 137 and 148 °C for **I**, between 132 and 138 °C for **II** and between 119 and 123 °C for **III**, ignoring the lower-melting polymorphs discussed below), while the clearing point of the SmA phases increases in a rather pronounced manner with chain length, the one exception being **II**$_{18}$ whose clearing point is lower than that of **II**$_{16}$. These observations suggest that the melting transition may well be controlled by some of the intermolecular interactions and ionic forces discussed above and that these can exert a great effect than that of chain length alone. However, chain length does control the stability of the liquid crystal mesophase and the fairly sharp increase in clearing point with *n* suggests that the increasing chain length helps to overcome the steric effect of the η^3-allyl group, which will act to reduce the overall anisotropy of the system.

Comparing the clearing points of the three series shows that those of the smallest anion (BF_4^-), **I**, are the highest while those of the largest anion ($CF_3SO_3^-$), **III**, are the lowest, which suggests that the anion size contributes negatively to the anisotropy of the materials.

Comparison between the thermal behaviour of these new complexes with the monosubstituted analogues,[19] [Pd(η^3-C_3H_5)(pz^{R}py)][X] is, unfortunately, not directly possible as the SmA phases of the latter were at rather high temperature and decomposition precludes a meaningful comparison. However we can deduce that the pz^{R2}py ligands have allowed us to obtain more stable mesophases upon complexation to [Pd(η^3-C_3H_5)]$^+$ than those with pz^{R}py.

An interesting feature of three of these complexes is the presence of more than one crystal polymorph in several samples. By this we do not refer to the various crystal–crystal transition mentioned in the text, rather the observation that some complexes (*e.g.* **II**$_{18}$) show melting points at two different temperatures (63 °C to SmA and 134 °C to isotropic for **II**$_{18}$). In **II**$_{14}$ and **II**$_{18}$, cold crystallisation of the SmA phases is observed when the phase forms from the lower-melting of the two solid phases, showing clearly that the higher-melting phase is thermodynamically more stable. Thus, the thermodynamically less stable phase is obtained from solution crystallisation. However, for **III**$_{18}$, the opposite seems to be true as the higher-melting solid phase is seen on first heating (Cr–I at 119 °C), while the lower-melting modification appears on second heating with no observed cold crystallisation (Cr–SmA at 52.5 °C). Thus, the liquid crystal range of these complexes is potentially rather wide, but is suppressed by the high melting point of the more thermodynamically stable crystal phase.

In order to confirm the smectic nature of the mesophases, X-ray diffraction experiments at variable temperature were undertaken for representative examples, namely **I**$_{18}$, **II**$_{18}$ and **III**$_{18}$.

The X-ray diffractograms for **I**$_{18}$ agree with the observations by POM, so that the sample enters to the mesophase between 135 and 140 °C and clears at slightly above 165 °C. On cooling the phase reappears at 162 °C, but crystallisation is not observed even at 50 °C. The pattern shown in Fig. 8 was recorded at 140 °C on heating the sample. Two, sharp, small-angle reflections were observed at 37.2 (d_{001}) and 18.5 (d_{002}) Å corresponding to a layered structure. In addition, a broad halo was located at 4.5 Å indicating the ligand-like order of the molten chains and thus a disordered phases. Furthermore, the lattice spacing is almost constant, changing by less than 5%, within the bounds of experimental error, with temperature.

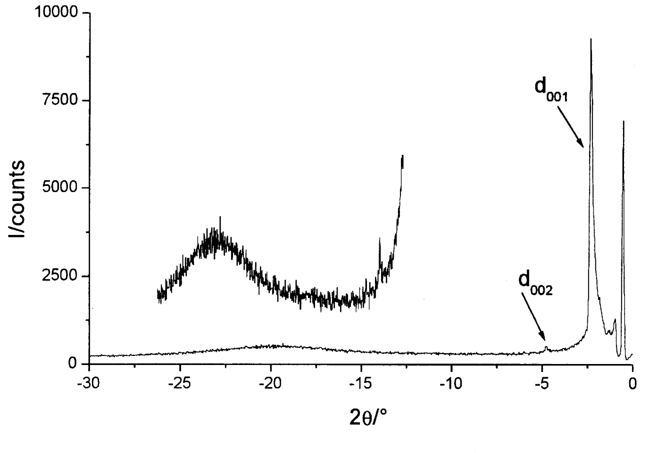

Fig. 8 X-Ray diffractogram of [Pd(η^3-C_3H_5)(pz^{odp2}py)][BF_4] (**I**$_{18}$) at 140 °C.

Similar patterns were recorded for **II**$_{18}$ and **III**$_{18}$, with spacing of d_{001} of 38.8 and 35.3 Å and d_{002} of 19.6 and 17.7 Å, respectively, with the broad halo at 4.4 Å (data taken from the diffractograms at 78 and 110 °C on cooling, respectively). However, the solidification of these compounds was observed at *ca.* 50 °C, and thus, the diffractogram at lower temperatures corresponds to a solid phase.

For $\mathbf{I}_{18}$, the length of the cationic part in the most extended crystalline conformation, calculated on the basis of the X-ray structure of $[Pd(\eta^3\text{-}C_3H_5)(pz^{bp2}py)][BF_4]$,[38] was estimated to be of *ca.* 68 Å, and the value of the spacing was 37.2 Å. Therefore these results suggest significant interdigitation of the layers. Similar features can also be suggested for $\mathbf{II}_{18}$ and $\mathbf{III}_{18}$.

An interesting comparison is that of the spacing (d_{001}) of related complexes containing mono or disubstituted pyrazole rings, *i.e.* $pz^{R}py$ and $pz^{R2}py$, and the same counteranion BF_4^-. So, d_{001} for $[Pd(\eta^3\text{-}C_3H_5)(pz^{hdp}py)][BF_4]$ (**V**) was 43.3 Å, and a molecular length, *l*, of *ca.* 34 Å was estimated in the fully extended configuration.[19] Because the *d* spacing was larger than *l* but smaller than 2*l*, an interdigitated bilayer structure related to that observed in the solid was proposed for these complexes (Fig. 4).[19] For $\mathbf{I}_{18}$, it is possible to suggest a similar structural arrangement, so that the molecular length of *ca.* 68 Å is now close to twice the observed *d*-spacing of 37.2 Å. Thus, we can confidently propose for $\mathbf{I}_{18}$ that the molecules are arranged in interdigitated bilayers and we note that such an arrangement exists also in the solid state (Fig. 4). Similar deductions can be made for complexes $\mathbf{II}_{18}$ and $\mathbf{III}_{18}$.

Conclusions

We have described the synthesis and thermal behaviour of a series of ionic palladium(II) allyl complexes bound to a series of difunctionalised pyrazolylpyridine ligands, $pz^{R2}py$. Consistent with their ionic nature, the complexes show SmA mesophases and the trends in transition temperature point to a crystalline phase who stability is determined largely by intermolecular Coulombic and hydrogen-bonding interactions. The stability of the mesophase, however, is governed first by the size of the anion (larger anions give less stable SmA phases) and by the length of the flexible alkyl chains (longer chains give more stable phases). An important feature of these materials is the crystalline polymorphism shown by some complexes so that some appear to show two melting points due to the metastability of the crystalline phase obtained from solution crystallisation.

Acknowledgements

We are grateful to the Dirección General de Investigación/MEC of Spain (Project No. BQU2003-07343) for financial support. We also thank to Comunidad de Madrid for financial support (Project GR/MAT/0511/2004) and the contract to M. C. T. We thank Dr B. Donnio (Institut de Physique et Chimie de Matériaux de Strasbourg IPCMS, Université de Strasbourg, France) for the X-ray diffraction experiments at variable temperature for compound $\mathbf{I}_{18}$ and for his helpful assessment in the interpretation of these XRD data.

References

1 J. L. Serrano, *Metallomesogens: Synthesis, Properties and Applications*, VCH, Weinheim, 1995.
2 B. Donnio and D. W. Bruce, *Struct. Bonding (Berlin)*, 1999, **95**, 193.
3 S. R. Collinson and D. W. Bruce, in *Transition Metals in Supramolecular Chemistry*, ed. J. P. Sauvage, Wiley, Chichester, 1999, ch. 7, p. 285.
4 B. Donnio, *Curr. Opin. Colloid Interface Sci.*, 2002, **7**, 371.
5 K. Binnemans and C. Görler-Walrand, *Chem. Rev.*, 2002, **102**, 2303.
6 B. Donnio, D. Guillon, R. Deschenaux and D. W. Bruce, *Comprehensive Coordination Chemistry II*, ed. J. A. McCleverty and T. J. Meyer, Elsevier, Oxford, UK, 2003, vol. 7, ch. 7.9, p. 357.
7 B. Donnio, D. Guillon, R. Deschenaux and D. W. Bruce, *Comprehensive Organometallic Chemistry III*, ed. R. H. Crabtree and D. M. P. Mingos, Elsevier, Oxford, UK, in press.
8 R. Deschenaux and J. W. Goodby, in *Ferrocene: Homogeneous Catalysis, Organic Synthesis, Materials Science*, ed. A. Togni and T. Hayashi, VCH, Weinheim, 1995, ch. 9, p. 471.
9 J. P. Rourke, F. P. Fanizzi, D. W. Bruce, D. A. Dunmur and P. M. Maitlis, *J. Chem. Soc., Dalton Trans.*, 1992, 3009.
10 (*a*) L. Ziminski and J. Malthête, *J. Chem. Soc., Chem. Commun.*, 1990, 1495; (*b*) P. Jacq and J. Malthête, *Liq. Cryst.*, 1996, **21**, 291.
11 E. Campillos, R. Deschenaux, A. M. Levelut and R. Ziessel, *J. Chem. Soc., Dalton Trans.*, 1996, 2533.
12 M. C. Torralba, M. Cano, J. A. Campo, J. V. Heras, E. Pinilla and M. R. Torres, *J. Organomet. Chem.*, 2001, **633**, 91.
13 M. C. Torralba, M. Cano, J. A. Campo, J. V. Heras, E. Pinilla and M. R. Torres, *J. Organomet. Chem.*, 2002, **654**, 150.
14 M. C. Torralba, M. Cano, J. A. Campo, J. V. Heras, E. Pinilla and M. R. Torres, *Inorg. Chem. Commun.*, 2002, **5**, 887.
15 M. C. Torralba, M. Cano, S. Gómez, J. A. Campo, J. V. Heras, J. Perles and C. Ruiz-Valero, *J. Organomet. Chem.*, 2003, **682**, 26.
16 M. C. Torralba, P. Ovejero, M. J. Mayoral, M. Cano, J. A. Campo, J. V. Heras, E. Pinilla and M. R. Torres, *Helv. Chim. Acta*, 2004, **87**, 250.
17 M. C. Torralba, M. Cano, J. A. Campo, J. V. Heras and E. Pinilla, *Z. Kristallogr.-New Cryst. Struct.*, 2005, **220**, 615.
18 M. J. Mayoral, M. C. Torralba, M. Cano, J. A. Campo and J. V. Heras, *Inorg. Chem. Commun.*, 2003, **6**, 626.
19 M. C. Torralba, M. Cano, J. A. Campo, J. V. Heras, E. Pinilla and M. R. Torres, *J. Organomet. Chem.*, 2006, **691**, 765.
20 M. Ghedini and A. Crispini, *Comments Inorg. Chem.*, 1999, **21**, 33.
21 M. Ghedini, D. Pucci, A. Crispini, I. Aiello, F. Barigelletti, A. Gessi and O. Francescangeli, *Appl. Organomet. Chem.*, 1999, **13**, 565.
22 J. Buey, G. A. Díez, P. Espinet, S. García-Granda and E. Pérez-Carreño, *Eur. J. Inorg. Chem.*, 1998, 1235.
23 M. J. Baena, J. Buey, P. Espinet and C. E. García-Prieto, *J. Organomet. Chem.*, 2005, **690**, 998.
24 L. Díez, P. Espinet, J. A. Miguel and M. P. Rodríguez-Medina, *J. Organomet. Chem.*, 2005, **690**, 261.
25 F. Neve, M. Ghedini and A. Crispini, *Chem. Commun.*, 1996, 2463.
26 F. Neve, M. Ghedini, A. Francescangeli and S. Campagna, *Liq. Cryst.*, 1998, **24**, 673.
27 D. Pucci, G. Barberio, A. Crispini, M. Ghedini and O. Francescangeli, *Mol. Cryst. Liq. Cryst.*, 2003, **395**, 155.
28 K. Binnemans, *Chem. Rev.*, 2005, **105**, 4148.
29 F. Neve, *Adv. Mater.*, 1996, **8**, 277.
30 M. Ghedini and D. Pucci, *J. Organomet. Chem.*, 1990, **395**, 105.
31 A. El-ghayoury, L. Douce, A. Skoulios and R. Ziessel, *Angew. Chem., Int. Ed.*, 1998, **37**, 1255.
32 D. W. Bruce, *Acc. Chem. Res.*, 2000, **33**, 831.
33 J. A. Campo, M. Cano, J. V. Heras, M. C. Lagunas, J. Perles, E. Pinilla and M. R. Torres, *Helv. Chim. Acta*, 2002, **85**, 1079.
34 F. Gómez-de la Torre, A. de la Hoz, F. A. Jalón, B. R. Manzano, A. Otero, A. M. Rodríguez and M. C. Rodríguez-Pérez, *Inorg. Chem.*, 1998, **37**, 6606.
35 F. Gómez-de la Torre, A. de la Hoz, F. A. Jalón, B. R. Manzano, A. M. Rodríguez, J. Elguero and M. Martínez-Ripoll, *Inorg. Chem.*, 2000, **39**, 1152.
36 J. Elguero, A. Fruchier, A. de la Hoz, F. A. Jalón, B. R. Manzano, A. Otero and F. Gómez-de la Torre, *Chem. Ber.*, 1996, **129**, 589.
37 F. A. Jalón, B. R. Manzano and B. Moreno-Lara, *Eur. J. Inorg. Chem.*, 2005, 100.
38 M. C. Torralba, M. Cano, J. A. Campo, J. V. Heras, E. Pinilla, M. R. Torres, J. Perles and C. Ruiz-Valero, *J. Organomet. Chem.*, 2006, **691**, 2614.